Journal of Hydrology 603 (2021) 126936

Contents lists available at ScienceDirect

Journal of Hydrology

journal homepage: www.elsevier.com/locate/jhydrol

BEST-WR: An adapted algorithm for the hydraulic characterization of hydrophilic and water-repellent soils

Simone Di Prima [a,b,*], Ryan D. Stewart [c], Majdi R. Abou Najm [d], Ludmila Ribeiro Roder [e,f], Filippo Giadrossich [a], Sergio Campus [a], Rafael Angulo-Jaramillo [b], Deniz Yilmaz [g], Pier Paolo Roggero [a], Mario Pirastru [a], Laurent Lassabatere [b]

[a] Department of Agricultural Sciences, University of Sassari, Viale Italia, 39A, 07100 Sassari, Italy
[b] Université de Lyon, UMR5023 Ecologie des Hydrosystèmes Naturels et Anthropisés, CNRS, ENTPE, Université Lyon 1, Vaulx-en-Velin, France
[c] School of Plant and Environmental Sciences, Virginia Polytechnic Institute and State University, Blacksburg, VA, United States
[d] Department of Land, Air and Water Resources, University of California, Davis, CA 95616, United States
[e] Department of Architecture, Design and Urban Planning, University of Sassari, Viale Piandanna, 4, 07100 Sassari, Italy
[f] School of Agriculture, São Paulo State University (UNESP), Fazenda Experimental Lageado, 18610-034 Botucatu, SP, Brazil
[g] Civil Engineering Department, Engineering Faculty, Munzur University, Tunceli, Turkey

ARTICLE INFO

This manuscript was handled by Corrado Corradini, Editor-in-Chief, with the assistance of Renato Morbidelli, Associate Editor

Keywords:
Soil water repellency
BEST
Water infiltration
Water retention
Hydraulic conductivity
Infiltrometer

ABSTRACT

Water-repellent soils usually experience water flow impedance during the early stage of a wetting process followed by progressive increase of infiltration rate. Current infiltration models are not formulated to describe this peculiar process. Similarly, simplified methods of soil hydraulic characterization (e.g., BEST) are not equipped to handle water-repellent soils. Here, we present an adaptation of the BEST method, named BEST-WR, for the hydraulic characterization of soils at any stage of water-repellency. We modified the Haverkamp explicit transient infiltration model, included in BEST for modeling infiltration data, by embedding a scaling factor describing the rate of attenuation of infiltration rate due to water repellency. The new model was validated using analytically generated data, involving soils with different texture and a dataset that included data from 60 single-ring infiltration tests. The scaling factor was used as a new index to assess soil water repellency in a Mediterranean wooded grassland, where the scattered evergreen oak trees induced more noticeable water repellency under the canopies as compared to the open spaces. The new index produced results in line with those obtained using the water drop penetration time test, which is one of the most widely test applied for quantifying soil water repellency persistence. Finally, we used BEST-WR to determine the hydraulic characteristic curves under both hydrophilic and hydrophobic conditions.

1. Introduction

The Beerkan Estimation of Soil Transfer parameters (BEST) method was proposed by Lassabatere et al. (2006) for the complete hydraulic characterization of soil, i.e., for estimating the soil water retention and hydraulic conductivity curves. The BEST method uses a single-ring infiltration experiment of the Beerkan type (Braud et al., 2005), in conjunction with other field and laboratory information. The method estimates the shape parameters of the characteristic curves via pedotransfer functions, using the textural information. Otherwise, the scale parameters are determined from the infiltration measurement. The BEST method has found a widespread application (Angulo-Jaramillo et al., 2019) and received recent methodological and theoretical developments by suggesting alternative algorithms to improve the procedure for fitting infiltration data (Bagarello et al., 2014b; Yilmaz et al., 2010) for the estimation of the soil sorptivity and the saturated soil hydraulic conductivity. Other studies aimed at adapting the BEST methods to other types of physical processes including sealing phenomena (Bagarello et al., 2014a) and dual-permeability soils (Lassabatere et al., 2019b). Although all these improvements allowed BEST to work satisfactorily in some non-ideal conditions, one challenge remained: to derive soil hydraulic parameters from convex cumulative infiltration curves, typical in water-repellent soils.

Soil water repellency (SWR) attenuates infiltration rates at early

* Corresponding author at: Department of Agricultural Sciences, University of Sassari, Viale Italia, 39A, 07100 Sassari, Italy.
E-mail address: sdiprima@uniss.it (S. Di Prima).

https://doi.org/10.1016/j.jhydrol.2021.126936
Received 4 June 2021; Received in revised form 4 September 2021; Accepted 7 September 2021
Available online 14 September 2021

time, thus generating convex-shaped cumulative infiltration curves, with an increasing slope with time. A practical implication of this mechanism is that water repellency can be easily detected by visually checking the shape of the cumulative infiltration curve (e.g., Alagna et al., 2019; Iovino et al., 2018; Lichner et al., 2013; Sándor et al., 2021). This led to infiltration data that is not consistent with the classical physics of infiltration and posed a challenge to the applicability of BEST under such conditions (Lassabatere et al., 2019a).

In this investigation, we present an adapted BEST method, named BEST-WR, for the hydraulic characterization of both hydrophilic and water-repellent soils. This method makes use of an empirical exponential scaling factor $(1-e^{-\alpha_{WR}t})$, recently proposed by Abou Najm et al. (2021), that describes the rate of attenuation of infiltration rate due to water repellency. This scaling factor can be used with any infiltration model (short-term, steady state, one-dimensional, two-dimensional, or three-dimensional). The correction factor accounts for the effect of time-varying water repellency at the soil surface without influencing the underlying physical model used, such that infiltration can still be quantified using common soil hydraulic properties (e.g., soil sorptivity and hydraulic conductivity). Here we modified the explicit transient infiltration model by Haverkamp et al. (1994), which is included in BEST for modeling infiltration data. The new BEST-WR method enables the hydraulic characterization of water-repellent soils and allows to successfully analyze heterogeneous datasets, including data collected under both hydrophilic and hydrophobic conditions. More precisely, the BEST-WR method provides the full set of unsaturated hydraulic parameters, i.e., the water retention and hydraulic conductivity curves plus the α_{WR} parameter that characterizes the degree of hydrophobicity of the tested soils. The BEST-WR method's ability to provide reliable soil hydraulic properties was then tested for both synthetic and real soils. To this aim, we first validated the infiltration model using analytically generated data involving soils with different texture, then with an infiltration dataset that included data from 60 field measurements. A further objective of the investigation was to assess SWR in a Mediterranean wooded grassland system by means of water drop penetration time and the new proposed scaling factor. Here the scattered evergreen oak trees were expected to induce SWR under the canopies, playing an important ecohydrological role and affecting water dynamics within the soil–vegetation atmosphere continuum.

2. Theory

The BEST method was developed by Lassabatere et al. (2006) to estimate parameters for the van Genuchten (1980) water retention curve, $\theta(h)$, with the Burdine (1953) condition, and the Brooks and Corey (1964) relationship for hydraulic conductivity, $K(\theta)$:

$$\theta(h) = \theta_s[1 + (\alpha_{vG}|h|)^n]^{-m} \tag{1a}$$

$$m = 1 - \frac{2}{n} \tag{1b}$$

$$K(\theta) = K_s\left(\frac{\theta}{\theta_s}\right)^{\eta} \tag{1c}$$

$$\eta = \frac{2}{nm} + 3 \tag{1d}$$

where h (L) is the water pressure head, α_{vG} (L^{-1}) is the van Genuchten pressure scale parameter, K_s (L T^{-1}) is the saturated hydraulic conductivity at the soil surface, θ_s (L^3 L^{-3}) is the saturated soil water content. Note that the case of a null residual soil water content corresponds to the case addressed by BEST methods (Angulo-Jaramillo et al., 2019). The shape parameters n, m and η are deduced from particle size distribution using specific pedo-transfer functions (PTF). More details on the estimation of these parameters can be found in Lassabatere et al. (2006) and Minasny and McBratney (2007) for an alternative estimation from the sandy, silty and clayey fractions. The K_s and α_{vG} parameters are derived from the analysis of cumulative water infiltration data.

For hydrophilic (i.e., non-water-repellent soils), the three dimensional (3D) cumulative infiltration, $I(t)$ (L), and infiltration rate, $i(t)$ (L T^{-1}), from a circular source under any zero or negative value of the pressure head can be approached by the following explicit transient and steady-state expansions (Haverkamp et al., 1994):

$$I(t) = S\sqrt{t} + (AS^2 + BK_s)t \tag{2a}$$

$$i(t) = \frac{S}{2\sqrt{t}} + (AS^2 + BK_s) \tag{2b}$$

$$I_{+\infty}(t) = (AS^2 + K_s)t + C\frac{S^2}{K_s} \tag{2c}$$

$$i_s = AS^2 + K_s \tag{2d}$$

where t (T) is the time elapsed since the start of the infiltration event, S (L $T^{-0.5}$) is the soil sorptivity, i_s (L T^{-1}) is the steady-state infiltration rate, B and C are coefficients that can be set equal to 0.467 and 0.639 for most soils with dry initial conditions (Bagarello et al., 2014c), and A (L^{-1}) is defined as follows:

$$A = \frac{\gamma}{r(\theta_s - \theta_i)} \tag{3}$$

where r (L) is the radius of the infiltration source, θ_i (L^3 L^{-3}) is the initial volumetric soil water content and γ is a shape parameter for geometrical correction of the infiltration front shape, which is commonly set to 0.75 (Haverkamp et al., 1994).

The BEST algorithm uses Eqs. (2a) and (2b) to model the transient cumulative infiltration and infiltration rate data. These equations are modified with the replacement of hydraulic conductivity as a function of sorptivity and the experimental steady-state infiltration rate, i_s^{exp} (L T^{-1}), using Eq. (2d), leading to:

$$K_s = i_s^{exp} - AS^2 \tag{4a}$$

$$I(t) = S\sqrt{t} + \left[A(1-B)S^2 + Bi_s^{exp}\right]t \tag{4b}$$

$$i(t) = \frac{S}{2\sqrt{t}} + \left[A(1-B)S^2 + Bi_s^{exp}\right] \tag{4c}$$

In this investigation we present an adapted BEST method, named BEST-WR, for the hydraulic characterization of water-repellent soils that can also be applied to hydrophilic soils. Using the correction factor, water infiltration into water-repellent soils can be modeled as follows (Abou Najm et al., 2021):

$$i_{WR}(t) = i(t)(1 - e^{-\alpha_{WR}t}) \tag{5}$$

where $i_{WR}(t)$ (L T^{-1}) is the scaled infiltration rate, $i(t)$ (L T^{-1}) is the unscaled infiltration rate that does not account for water repellency, and $(1-e^{-\alpha_{WR}t})$ is the exponential scaling factor, in which the empirical parameter α_{WR} (T^{-1}) is considered to reflect the rate of water repellency attenuation during infiltration (Abou Najm et al., 2021).

Here we combine Eqs. (4c) and (5), resulting in the following expression for transient infiltration in a water-repellent soil:

$$i_{WR}(t) = i(t)(1 - e^{-\alpha_{WR}t}) = \left\{\frac{S}{2\sqrt{t}} + \left[A(1-B)S^2 + Bi_s^{exp}\right]\right\}(1 - e^{-\alpha_{WR}t}) \tag{6}$$

Cumulative infiltration, I_{WR} (L), is then found by integrating Eq. (6) with respect to time, between 0 and any time, t, as suggested by Abou Najm et al. (2021):

Table 1
Soil hydraulic parameters for the six studied soils used to model the infiltration experiments, originally from Carsel and Parrish (1988).

Soil texture	Sand	Loamy Sand	Sandy Loam	Loam	Silt Loam	Silty Clay Loam
θ_r	0.045	0.057	0.065	0.078	0.067	0.089
θ_s	0.43	0.41	0.41	0.43	0.45	0.43
α_{vG} (mm^{-1})	0.0145	0.0124	0.0075	0.0036	0.002	0.001
n	2.68	2.28	1.89	1.56	1.41	1.23
K_s (mm h^{-1})	297.0	145.9	44.2	10.44	4.5	0.7
l	0.5	0.5	0.5	0.5	0.5	0.5

$$I_{WR}(t) = S\sqrt{t} - \frac{S\sqrt{\pi}}{2\sqrt{\alpha_{WR}}} erf(\sqrt{\alpha_{WR} t}) + \left[A(1-B)S^2 + Bi_s^{exp}\right]t - \frac{\left[A(1-B)S^2 + Bi_s^{exp}\right](1-e^{-\alpha_{WR} t})}{\alpha_{WR}} \quad (7)$$

where *erf* is the error function assessed between the lower and upper integration limits.

Eq. (7), when fitted to experimental data, has only two unknown parameters: α_{WR} and S. In comparison, the examples in Abou Najm et al. (2021) fit the model with three unknown parameters (α_{WR}, S, and a parameter related to K_s). Thus, Eq. (7) is more likely to identify unique parameters when analysed using classical least squares optimization. Then, the other hydraulic parameters (related to the water retention and the hydraulic conductivity curves) are estimated as in BEST slope method (Lassabatere et al., 2006).

3. Material and methods

3.1. Analytical validation

We assessed the accuracy of the proposed infiltration model (Eq.(7)) for six soils, with regularly shaped, convex $I(t)$ curves, using synthetic soils previously characterized by Di Prima et al. (2020) and Hinnell et al. (2009): sand, loamy sand, sandy loam, loam, silt loam, silty clay loam. These soils were chosen to cover a wide range of hydraulic responses without water repellency. We modelled infiltration experiments for these synthetic hydrophilic soils using the model proposed by Smettem et al. (1994):

$$I(t) = I_{1D}(t) + \frac{\gamma S^2}{r\Delta\theta} \quad (8)$$

where $\Delta\theta = (\theta_s - \theta_i)$, I (L) is the 3D cumulative infiltration and I_{1D} (L) is the 1D cumulative infiltration into uniform, initially unsaturated soil profiles. Here we modelled I_{1D} using the following implicit equation (Haverkamp et al., 1990):

$$\frac{2\Delta K^2}{S^2} t = \frac{1}{1-\beta}\left[\frac{2\Delta K}{S^2}(I_{1D}(t) - K_i t) - ln\left(\frac{exp\left(2\beta\frac{\Delta K}{S^2}(I_{1D}(t) - K_i t)\right) + \beta - 1}{\beta}\right)\right] \quad (9)$$

where K_i (L T^{-1}) is the initial soil hydraulic conductivity, $\Delta K = (K_s - K_i)$, and β is a shape parameter related to water diffusivity that is commonly set equal to 0.6 (Haverkamp et al., 1994).

The synthetic curves were modelled considering an initially dry condition, with an initial value of the saturation degree, *Se*, of 0.1. This value was converted to the equivalent θ_i value for each soil using the relationship $Se = (\theta_i - \theta_r)/(\theta_s - \theta_r)$. We considered the θ_r values from Table 1 for computing the sorptivity and modelling the synthetic curves. The sorptivity was then estimated as follows (Parlange, 1975):

$$S = \sqrt{\int_{h(\theta_i)}^{0} (\theta_s + \theta(h) - 2\theta_i) K(h) dh} \quad (10)$$

The integral in Eq. (10) was computed using the intg function defined in Scilab (Campbell et al., 2010) and validated against the new procedure proposed by Lassabatere et al. (2021). The water retention curve and the hydraulic conductivity functions were calculated according to the van Genuchten–Mualem model (Mualem, 1976; van Genuchten, 1980). Hydraulic parameters for the six synthetic soils were taken from Carsel and Parrish (1988) (Table 1). Default values of $\beta = 0.6$ and $\gamma = 0.75$ were assumed, as commonly suggested by many investigations (Angulo-Jaramillo et al., 2019). To ensure steady-state conditions, each infiltration process was modelled for a period three times longer than the maximum time for which Eqs. (2a) and (2b) are considered valid (Haverkamp et al., 1994), with t_{max} (T) calculated as follows (Lassabatere et al., 2006):

$$t_{max} = \frac{1}{4(1-B)^2}\left(\frac{S}{K_s}\right)^2 \quad (11)$$

For the generation of the cumulative infiltrations for the water repellent soils, we extended the quasi-exact implicit (QEI) model developed by Haverkamp et al. (1990) to water repellent soils. At this aim, we considered the integration of the corrected infiltration (Eq. (5)):

$$I_{WR}(t) = \int_0^t i(\bar{t})\left(1 - e^{-\alpha_{WR}\bar{t}}\right) d\bar{t} \quad (12)$$

The Eq. (12) was simplified considering integration by parts and algebraic operations to relate the cumulative infiltration corrected for water repellency, $I_{WR}(t)$, with the cumulative infiltration of the same soil without water repellency, $I(t)$, leading to:

$$I_{WR}(t) = (1 - e^{-\alpha_{WR} t}) I(t) - \alpha_{WR} \int_0^t e^{-\alpha_{WR}\bar{t}} I(\bar{t}) d\bar{t} \quad (13)$$

For the computation of Eq. (13), we injected synthetic curves, $I(t)$, into Eq. (13) to compute the cumulative infiltration for the same soils with water repellency, $I_{WR}(t)$. The empirical parameter α_{WR} was varied from 0.04 to 10000 h^{-1} depending on the type of soil to cover the whole range of shapes from regular concave to convex with an inflection point. Regarding time set, the final time was set as the maximum time between 3 t_{max} and the time t_{rec} needed to recover 95% of the regular infiltration rate, i.e., so that $(1 - e^{-\alpha_{WR} t}) = 0.95$. Indeed, if such a time is not reached, the infiltration rate $i_{WR}(t)$ continues to increase, the steady state is not reached and the operator should continue the experiment on the field.

The two sets of infiltration data obtained for hydrophilic soils, $I(t)$, and water-repellent soils, $I_{WR}(t)$, were treated with the new algorithm BEST-WR. At first, the criterion suggested by Bagarello et al. (1999) was used to separate the transient and steady-state conditions for cumulative infiltration data. We conducted a linear regression analysis for the last three data points of $I(t)$ versus t. Then, the time to steady-state, t_s (L), was determined as the first value for which:

$$\widehat{E} = \left|\frac{I(t) - I_{reg}(t)}{I(t)}\right| \leq E \quad (14)$$

Table 2

Reference values (α_{WR}, S and K_s), BEST-WR ($\widehat{\alpha}_{WR}$, $\widehat{S}_{WR}$ and $\widehat{K}_{s,WR}$) and BEST ($\widehat{S}$ and $\widehat{K}_s$) estimations, and fit relative errors ($Er_{FIT,WR}$ and Er_{FIT}) for the six synthetic soils. The values of the initial volumetric soil water content (θ_i) and the slope (i_s^{exp}) and intercept (b_s^{exp}) of the linear regression fitted to the steady-state portion of the curves are also reported.

Soil	θ_i	S	K_s	α_{WR}	i_s^{exp}	b_s^{exp}	BEST-WR (Eq. (7))				BEST (Eq. (4b))		
							$\widehat{\alpha}_{WR}$	$\widehat{S}_{WR}$	$\widehat{K}_{s,WR}$	$Er_{FIT,WR}$	$\widehat{S}$	$\widehat{K}_s$	Er_{FIT}
	[m^3 m^{-3}]	[mm $h^{-0.5}$]	[mm h^{-1}]	[h^{-1}]	[mm h^{-1}]	[mm]	[h^{-1}]	[mm $h^{-0.5}$]	[mm h^{-1}]	[%]	[mm $h^{-0.5}$]	[mm h^{-1}]	
Sand	0.083	86.5	297.0	*	523.99	13.5	15,660	90.8	285.8	0.3	89.1	295.0	0.6
				10,000**	523.97	12.7	3486	90.9	285.8	0.3	87.0	305.8	1.1
				1000	523.97	10.8	737	90.9	285.5	0.3	81.6	331.9	2.6
				800	523.97	10.4	612	91.0	285.2	0.3	80.5	336.8	2.9
				600	523.97	9.8	479	91.0	284.8	0.3	79.0	344.0	3.4
				400	523.97	8.8	335	91.2	284.0	0.3	76.2	356.6	4.2
				200	523.49	6.4	175	91.9	280.0	0.2	70.0	382.3	6.0
				100	523.49	2.3	91	92.7	275.3	0.1	58.6	424.3	8.6
				80	523.47	0.5	73	93.2	272.8	0.1	53.6	440.5	9.6
				60	522.92	−2.3	55	94.2	266.8	0.1	47.5	457.9	10.6
				40	521.94	−7.5	36	95.8	257.1	0.0	31.1	494.1	12.3
Loamy sand	0.092	58.2	145.9		258.07	12.5	8367	61.1	140.4	0.3	60.0	144.9	0.6
				5000	257.87	11.7	1797	61.1	140.2	0.3	58.5	150.3	1.1
				500	257.87	9.8	373	61.2	140.1	0.3	54.7	163.6	2.7
				400	257.87	9.5	309	61.2	140.0	0.3	54.0	166.1	3.0
				300	257.87	8.9	241	61.3	139.7	0.3	52.9	169.8	3.5
				200	257.87	8.0	168	61.4	139.3	0.3	50.9	176.3	4.4
				100	257.64	5.6	88	61.8	137.3	0.2	46.6	189.4	6.2
				50	257.64	1.7	45	62.5	134.8	0.1	38.6	210.8	8.9
				40	257.63	−0.1	37	62.8	133.5	0.1	35.1	218.9	9.8
				30	257.33	−2.8	27	63.5	130.3	0.1	30.8	227.6	10.8
				20	256.60	−7.8	18	64.7	125.0	0.0	18.2	246.2	12.5
Sandy loam	0.100	36.0	44.2		87.71	15.7	2637	37.5	42.4	0.2	36.9	43.8	0.5
				1000	87.75	14.6	434	37.5	42.4	0.2	36.0	46.0	1.1
				100	87.67	12.0	79	37.6	42.0	0.3	33.7	51.1	2.8
				80	87.67	11.4	65	37.7	42.0	0.2	33.2	52.1	3.2
				60	87.67	10.6	50	37.7	41.9	0.2	32.5	53.6	3.7
				40	87.67	9.1	35	37.8	41.7	0.2	31.2	56.3	4.7
				20	87.67	5.4	18	38.0	41.3	0.2	27.8	62.8	6.9
				10	87.60	−0.7	9	38.4	40.0	0.1	22.7	71.0	9.5
				8	87.58	−3.5	7	38.6	39.5	0.1	20.2	74.4	10.5
				6	87.53	−7.9	6	39.0	38.6	0.0	15.8	79.5	11.8
				4	86.41	−14.7	4	40.0	34.8	0.0	5.1	85.6	12.7
Loam	0.113	20.9	10.4		24.57	22.2	605	21.5	9.9	0.2	21.3	10.3	0.4
				100	24.52	20.2	58	21.5	9.9	0.2	20.6	11.1	1.2
				10	24.50	14.6	9	21.6	9.8	0.2	18.9	13.2	3.6
				8	24.50	13.5	7	21.6	9.8	0.2	18.5	13.7	4.1
				6	24.50	11.7	5	21.6	9.7	0.2	17.9	14.3	4.8
				4	24.50	8.4	4	21.7	9.7	0.1	16.9	15.5	6.1
				2	24.48	−0.1	2	21.9	9.4	0.1	14.3	18.0	8.6
				1	24.45	−14.9	1	22.2	9.0	0.0	9.2	21.8	11.8
				0.8	24.30	−20.7	0.8	22.3	8.5	0.0	2.0	24.2	12.5
Silt loam	0.105	16.3	4.5		12.41	31.1	251	16.7	4.3	0.2	16.6	4.4	0.3
				80	12.40	29.6	35	16.8	4.3	0.2	16.3	4.7	0.7
				8	12.40	25.0	6	16.8	4.3	0.2	15.6	5.3	2.0
				6.4	12.40	24.1	5.3	16.8	4.3	0.2	15.5	5.4	2.3
				4.8	12.40	22.7	4.1	16.8	4.2	0.2	15.3	5.6	2.7
				3.2	12.40	20.2	2.8	16.8	4.2	0.2	14.9	6.0	3.4
				1.6	12.40	13.7	1.5	16.8	4.2	0.1	13.8	6.9	5.2
				0.8	12.40	2.9	0.8	16.9	4.1	0.1	12.2	8.1	7.5
				0.64	12.40	−2.1	0.6	16.9	4.1	0.1	11.4	8.6	8.5
				0.48	12.40	−10.2	0.5	17.0	4.0	0.0	10.1	9.4	9.8
				0.32	12.38	−25.1	0.3	17.1	3.9	0.0	7.4	10.8	11.7
Silty clay loam	0.123	6.0	0.7		1.89	27.0	38	6.1	0.7	0.2	6.1	0.7	0.3
				10	1.90	25.2	5	6.1	0.7	0.2	6.0	0.7	0.9
				1	1.90	20.2	0.8	6.1	0.7	0.2	5.6	0.9	2.5
				0.8	1.90	19.2	0.7	6.1	0.7	0.2	5.6	0.9	2.8
				0.6	1.90	17.7	0.5	6.2	0.7	0.2	5.5	0.9	3.3
				0.4	1.90	14.9	0.4	6.2	0.7	0.1	5.3	1.0	4.3
				0.2	1.90	7.6	0.2	6.2	0.7	0.1	4.7	1.2	6.5
				0.1	1.89	−4.8	0.1	6.2	0.6	0.1	3.9	1.4	9.2
				0.08	1.89	−10.6	0.08	6.2	0.6	0.0	3.5	1.5	10.2
				0.06	1.89	−19.8	0.06	6.3	0.6	0.0	2.8	1.6	11.6
				0.04	1.87	−34.5	0.04	6.4	0.5	0.0	1.1	1.8	12.8

* For each soil type, the parameters of the first row are representative of the curves generated by Eqs. (8) and (9).

** All the other rows refer to Eq. (13).

Table 3
Sample size (N), minimum (min), maximum (max), mean and coefficient of variation (CV, %) of the % clay (0–2 μm), % silt (2–50 μm), and % sand (50–2000 μm) content (size classes based on USDA classification system) in the 0–10 cm depth range, dry soil bulk density (ρ_b), and initial volumetric soil water content (θ_i), measured below the tree canopies and in the open spaces at the Berchidda site (sample size for each variable and location, $N = 9$).

Variable	Location	min	max	mean	CV
Clay (%)	Open space	3.7	9.7	8.2	23.6
	Below tree canopy	3.6	8.6	5.8	27.3
Silt (%)	Open space	11.5	16.0	13.9	11.4
	Below tree canopy	8.8	19.2	14.3	23.8
Sand (%)	Open space	74.2	84.8	77.9	4.2
	Below tree canopy	76.1	86.0	79.9	5.0
ρ_b (g cm^{-3})	Open Space	1.436	1.662	1.551	3.9
	Below tree canopy	1.212	1.446	1.354	5.8
θ_i (m^3 m^{-3})	Open Space	0.065	0.147	0.099	24.6
	Below tree canopy	0.086	0.177	0.138	19.3

where $I_{reg}(t)$ is estimated from regression analysis, and E defines a given threshold to check linearity. Eq. (14) was applied from the start of the experiment until finding the first data point that fits the condition $\widehat{E} \leq E$ (Angulo-Jaramillo et al., 2016). The commonly used value of $E = 2\%$ was adopted in this investigation.

The slope, i_s^{exp} (L T^{-1}), was estimated by linear regression analysis of steady-state data (i.e., all data points measured after time t_s, when $\widehat{E} \leq 2$). Then, the estimators for S and α_{WR}, $\widehat{S}$ and $\widehat{\alpha}_{WR}$, were obtained fitting the transient portion of the synthetic data (i.e., data points from time 0 until time t_s, when $\widehat{E} > 2$) to Eq. (7) by minimizing the sum of square of errors (SSE) between synthetic data and modeled cumulative infiltration. The optimization was carried out with 25 sets of initial parameter values for $\widehat{S}_{WR}$, and $\widehat{\alpha}_{WR}$, using the following starting values: $\widehat{S}_{WR}$ = 0.001, 0.01, 0.1, 1, and 10 mm h$^{-0.5}$, and $\widehat{\alpha}_{WR} = 0.001$, 0.01, 0.1, 1, and 10 h^{-1}. The parameter set with the smallest SSE was chosen as the global optimum solution. The estimator for K_s, $\widehat{K}_{s,WR}$, was estimated via Eq. (4a). For comparison, we also analyzed the data using Eq. (4b). This comparison was aimed to highlight contrasting fitting abilities between the two models (adapted to water repellency, Eq. (7), and the regular BEST method, Eq. (4b)) when analyzing data affected by water repellency. Thus, we obtained two estimations for soil sorptivity, namely $\widehat{S}_{WR}$ from Eq. (7) and $\widehat{S}$ from Eq. (4b), leading to two estimations for the saturated soil hydraulic conductivity ($\widehat{K}_{s,WR}$and $\widehat{K}_s$) from Eq. (4a).

The accuracy of these fits was assessed on the basis of the consistency of the model shape and the fit relative error, Er_{FIT}, estimated as follows:

$$Er_{FIT} = \sqrt{\frac{\sum_{i=1}^{k}\left[I_{exp}(t_i) - I_{est}(t_i)\right]^2}{\sum_{i=1}^{k} I_{exp}^2(t_i)}} \quad (15)$$

where k is the number of data points considered for the transient state and I_{exp} and I_{est} are the experimental and estimated values for water infiltration.

Relative error, Er, was also calculated for each estimated value for $\widehat{\alpha}_{WR}$, soil sorptivity ($\widehat{S}_{WR}$ and $\widehat{S}$) and saturated soil hydraulic conductivity ($\widehat{K}_{s,WR}$and $\widehat{K}_s$) compared to the corresponding reference value (i.e., α_{WR}, S and K_s) as follows:

$$Er(x) = \frac{\widehat{x} - x}{x} \quad (16)$$

where $\widehat{x}$ is the estimated value and x is the target, i.e., the reference value α_{WR}, S and K_s (Table 2). According to the accuracy criterion by Reynolds (2013), the estimates were deemed accurate when they fell within the range $0.75 \leq \widehat{x}/x \leq 1.25$ (i.e. $|Er(x)| \leq 25\%$ error). This stringent criterion was used because the parameters were estimated by analytically generated data, and therefore were free of the perturbations embedded in field and laboratory measurements (e.g., measurement error, random noise and natural variability).

3.2. Experimental site

The Berchidda site (40°48′57.28″N, 9°17′33.09″E) is a Mediterranean wooded grassland system with herbaceous grasslands dominated by annual species and scattered evergreen oak trees (*Quercus suber* L. and *Quercus ilex* L.), located in the Long Term Observatory of Berchidda-Monti in NE Sardinia, Italy (Bagella et al., 2020). The site is representative of agro-silvo-pastoral systems widespread in the Mediterranean basin, in particular within the Iberian Peninsula (Lozano-Parra et al., 2015). The mean annual rainfall is 632 mm, of which 70% occurs during October to May. The mean annual temperature is 14.2 °C. According to the USDA standards, the sampled soils of the upper horizon ranged in texture from sandy loam to loamy sand (Typic Dystroxerept) (Table 3). The natural potential vegetation is mainly represented by cork oak forests, also referred to as the *Viola dehnhardtii-Quercetum suberis* association (Bagella et al., 2016).

3.3. Automated single-ring infiltration test

Sixty single-ring infiltration tests were performed at randomly selected sampling points in correspondence of three selected trees: thirty below tree canopies (ten below each tree), and another thirty in the open grasslands (ten in the proximity of each tree, in the open spaces). For each sampling point, the litter and leaf residues were gently removed from the soil surface and a stainless steel ring with a 15-cm inner diameter was inserted shallowly into the soil according to the Beerkan procedure for single-ring infiltration experiments (Lassabatere et al., 2006). The tests were carried out using the automated single-ring infiltrometer proposed by Concialdi et al. (2020) to infiltrate a total cumulative infiltration of 280 mm, assuming an infiltration surface of 94 cm^2. The devices were equipped with differential transducers to measure the drop of water level in the Mariotte reservoirs (see Fig. 1 in Concialdi et al. 2020). To setup the experiment, we followed the procedure described in Di Prima (2015) and Di Prima et al. (2016). We firstly positioned a plastic film on the soil surface inside the ring and applied a small water head of few mm, depending on the surface roughness and never exceeding 10 mm. The infiltrometer was positioned inside the ring and regulated in height so that the base was in contact with the ponded water. The data acquisition started after the Mariotte bottle was filled with water and activated. Finally, the infiltration experiment started when the plastic film was removed. The automated procedure proposed by Concialdi et al. (2020) to treat the transducer output was subsequently applied to determine the cumulative infiltration curves. A video tutorial showing the field procedure and the data processing can be viewed online (Di Prima, 2019). For each site, undisturbed soil cores (50 mm in height and 50 mm in diameter) were collected at randomly sampled points and used to determine both the soil bulk density, ρ_b (g cm^{-3}), and the initial volumetric soil water content, θ_i (cm^{3}cm^{-3}). Disturbed soil samples were also collected to determine the particle size distribution (PSD) (Gee and Bauder, 1986). The measured soil physical properties are summarized in Table 3.

All the experimental infiltration curves were analyzed using the same procedure described above for the synthetic data. In addition, we followed Lassabatere et al. (2006)) and used the S_{WR} and $K_{s,WR}$ estimations in conjunction with the PSD to calculate the van Genuchten scale parameter, $\alpha_{vG,WR}$, values (see Eq. (22) in Lassabatere et al. (2006)).

3.4. Water drop penetration time (WDPT) test

The water drop penetration time (WDPT) test (Wessel, 1988) was aimed at characterizing contrasting responses in terms of soil surface

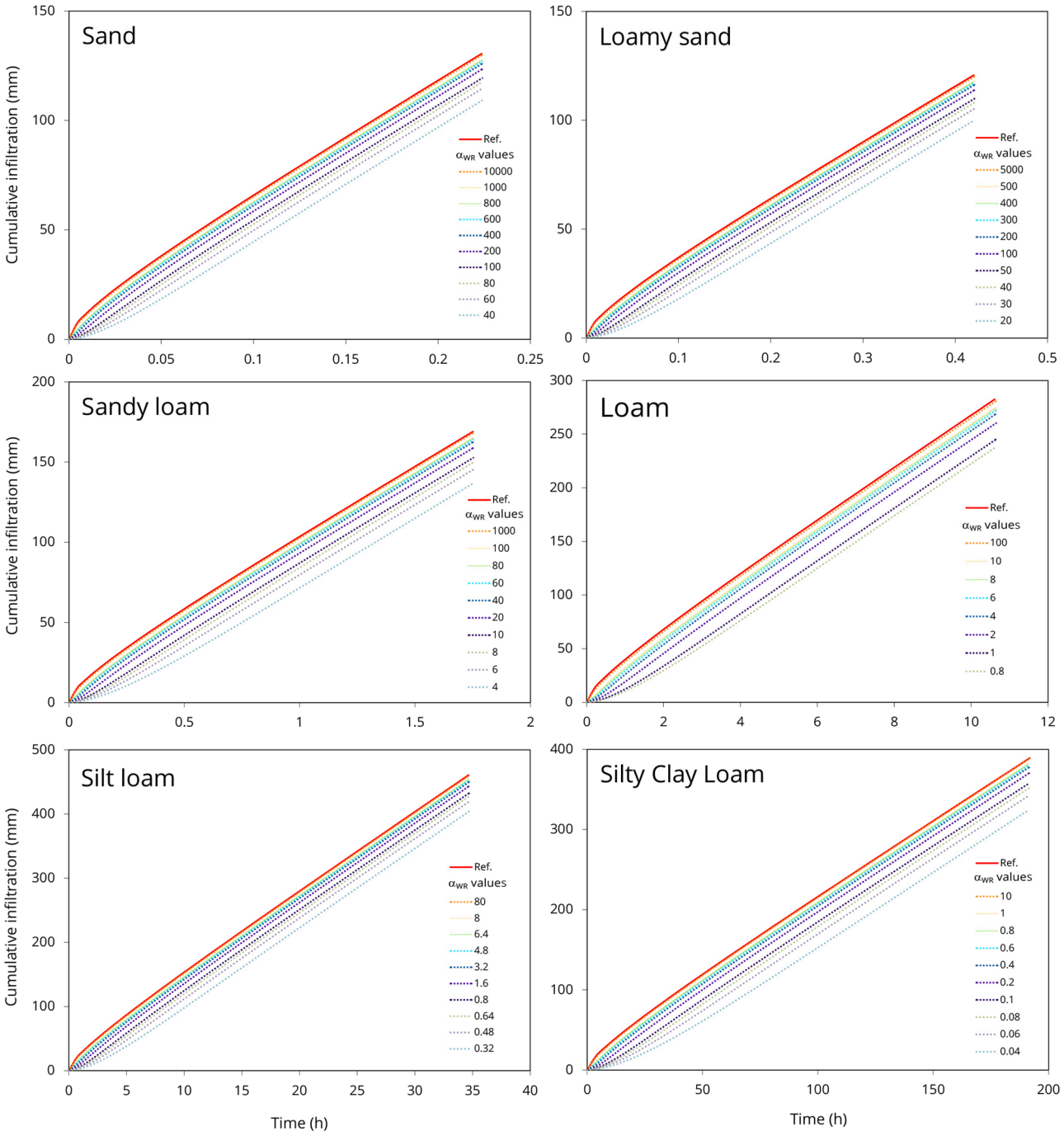

Fig. 1. Cumulative infiltration curves for different synthetic soils. The reference curves (in red) were generated analytically using Eqs. (8) and (9) and the parameters listed in Table 1. All the other curves were generated analytically using Eq. (13), and assuming an α_{WR} value raging from 0.04 to 10000 h^{-1}, depending on the soil. (For interpretation of the references to colour in this figure legend, the reader is referred to the web version of this article.)

wettability between two contrasting situations, i.e., below the tree canopies and in open spaces. This method is one of the most widely applied for quantifying SWR persistence (Doerr et al., 2000). WDPT tests were conducted at the three selected trees with nine tests below tree canopies and other nine in open spaces. For each sampling point, the litter and leaf residues were gently removed from the soil surface and ten drops (0.05 mL) of distilled water were placed using a pipette onto the soil surface at a small distance (i.e., a few cm) one to another and measuring the actual time until complete infiltration of each drop. The recorded time was stopped after 3600 s, although some drops did not infiltrate during this time interval. In such cases, a WDPT value of 3600 s was assigned (Buczko et al., 2006). Thus, we measured the infiltration of 180 drops, ninety below the tree canopies and other ninety in the open spaces. For each situation, a representative WDPT value was obtained by averaging the ninety WDPT measurements.

4. Results and discussion

4.1. Analytical validation for six synthetic soils

When cumulative infiltration was calculated for all synthetic soils without water repellency (Table 2) using Eqs. (8) and (9), all curves exhibited a concave shape as a function of time, typical for hydrophilic soils (Fig. 1, red reference curves). As the process approached steady

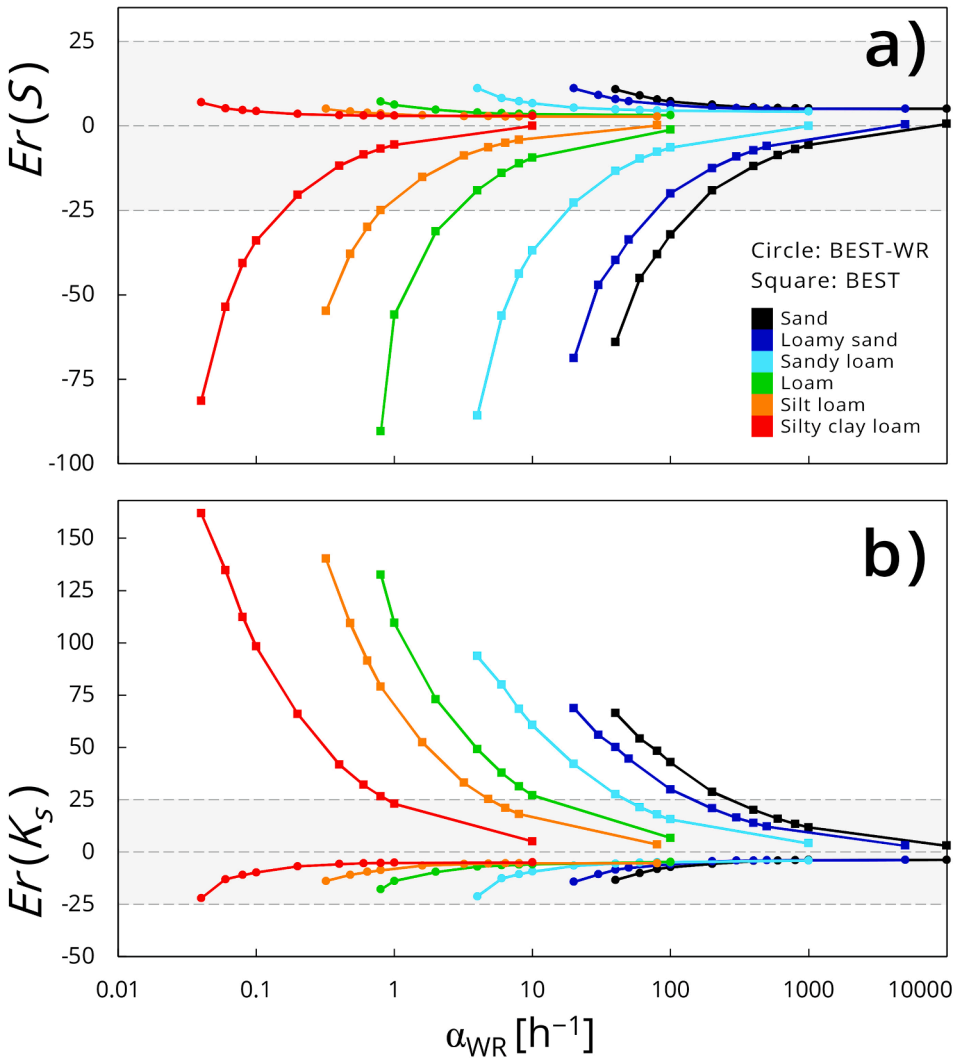

Fig. 2. Relative error of the estimated values for (**a**) soil sorptivity, S, and (**b**) saturated soil hydraulic conductivity, K_s, for six synthetic soils. Circles and squares indicate respectively BEST-WR and BEST estimations.

state, cumulative infiltration curves became approximately linear with time. This behaviour is well known for hydrophilic soils and shows how the influence of capillarity decreases as the wetting front moves away from the source and the hydraulic gradient decreases (Xu et al., 2012).

When cumulative infiltration was calculated using Eq. (13) to include water repellency, the curves exhibited a concave shape for higher α_{WR} values and a convex shape for lower α_{WR} values (Fig. 1), the latter being typical of water-repellent soils. These shapes are in line with observed water infiltrations into water-repellent soils. Convex shapes may be explained as follows. When water infiltrates into these soils, the advance of water during the early phase of wetting is impeded owing to hydrophobic surface films on soil particles, resulting in a contact angle higher than 90° between soil and water (Jarvis et al., 2008). In addition, the hydrophobic material is often heterogeneously distributed, leading to a fractional wettability of the bulk media and the concomitance of contrasting factors that simultaneously tends to increase and decrease infiltration rates (Beatty and Smith, 2013). As a consequence, the final shape of the cumulative infiltration curve is the result of the relative importance during the infiltration process of water repellency, which triggers an increase in the infiltration rate over time, and the usual gravity and capillarity driven flow with decreasing infiltration rate over time until the attainment of steady state. Our model (Eq. (13)) reproduced these trends. In addition, we note that for the highest α_{WR} values the curves generated using Eq. (13) are almost identical with the reference curves generated using the Haverkamp Eqs. (8) and (9). This clearly points to the ability of Eq. (13) to accurately calculate cumulative infiltration also for the case of hydrophilic soils, provided that values of α_{WR} were chosen large enough. The proposed model (Eq. (13)) is then consistent with the modelling of both hydrophilic soils (no water repellency) and water repellent soils.

For the treatment of the synthetic data with BEST-WR, we first determined the time to steady-state, t_s, with the condition $\widehat{E} > 2$. This threshold split the synthetic data into two subsets: a transient phase (i.e., when $\widehat{E} > 2$), and a steady-state phase (i.e., when $\widehat{E} \leq 2$). We estimated from the steady-state portion the value of the linear regression model slope, i_s^{exp}, and intercept, b_s^{exp} (mm). Note that flow impediment at the beginning of the infiltration experiment leads convex-shaped curves and therefore to negative b_s^{exp} values (Table 2). Thus, negative values of this parameter can be considered indicative of the occurrence of water repellency phenomena, although other factors could also play some role, such as heterogeneous soil structure, changes in soil structure during the infiltration run, air-entrapment, heterogeneous profiles for initial soil moisture and temperature (e.g., Loizeau et al., 2017).

Then, Eqs. (7) and (4b) were fitted to the transient portion of the curve using i_s^{exp} and optimizing $\widehat{\alpha}_{WR}$ and $\widehat{S}_{WR}$ for Eq. (7), and $\widehat{S}$ for Eq. (4b) before deriving $\widehat{K}_{s,WR}$ and $\widehat{K}_s$ with Eq. (4a). The fitting of Eq. (7) to transient data was accurate with $Er_{FIT,WR}$ values never exceeding 0.3%

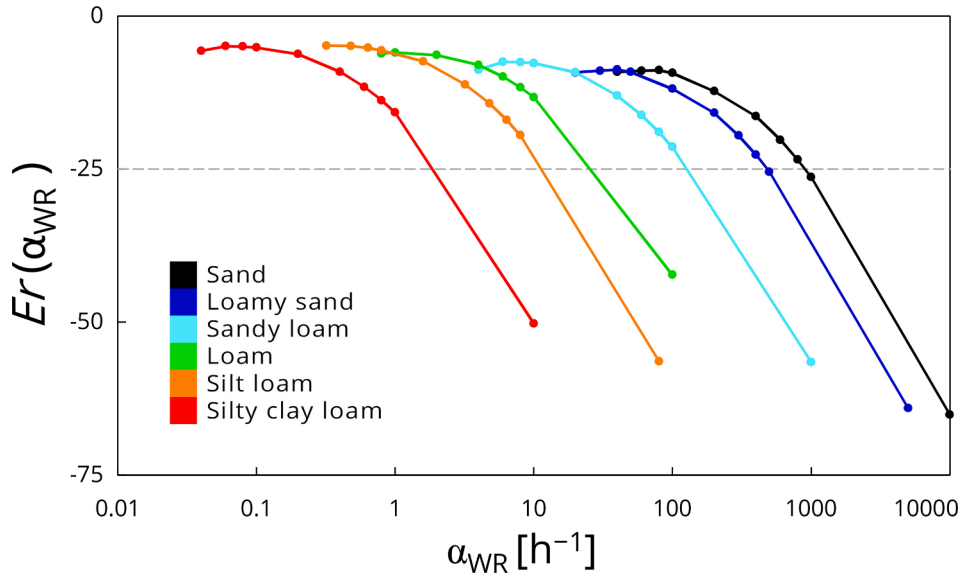

Fig. 3. Relative error of the α_{WR} parameter for six synthetic soils.

(Table 2). On the other hand, less accurate fits were found for Eq. (4b), with increasing Er_{FIT} values for decreasing α_{WR} (more convex curves), and values ranging from 0.3 to 12.8%. More specifically, 45.3% of Er_{FIT} values were higher than 5%, that is commonly considered the threshold for accurate fits. Regarding the quality of estimates, relative error, $Er(S)$ and $Er(K_s)$, between estimated ($\widehat{S}_{WR}$ and $\widehat{K}_{s,WR}$) and reference (S and K_s) values ranged from − 22.1 to 11.1% (circle symbols in Fig. 2), indicating that all $\widehat{S}_{WR}$ and $\widehat{K}_{s,WR}$ values were accurate based on our stated criterion ($Er < 25\%$). However, the errors always increased for decreasing α_{WR} values. We therefore argue that the soil hydraulic properties may be misestimated in case of very low α_{WR} values, namely for extremely convex-shaped curves. In this case, BEST-WR is expected to overestimate S and consequently to underestimate K_s. Regarding the α_{WR} parameter, $Er(\alpha_{WR})$, ranged from − 65.1 to 4.8% (Table 2). Most of the estimations were below the selected threshold of 25%, although, for each synthetic soil, the one or two highest α_{WR} yielded $|Er(\alpha_{WR})|$ values higher than 25% (Fig. 3). However, this parameter is expected to have a less relevant effect on the estimation of the soil parameters (S and K_s) when it assumes very high values. Indeed, the lowest errors for S and K_s were found for high α_{WR} values (Fig. 2). In other words, we gain in accuracy for S and K_s for moderate or light water repellency, and for α_{WR} for strong water repellency. In all cases, the parameters easier to estimate are those that have a relevant impact on the cumulative infiltration.

For BEST (Eq. (4b)), relative error between estimated ($\widehat{S}$ and $\widehat{K}_s$) and reference (S and K_s) values ranged from − 90.5 to 161.9% (square symbols in Fig. 2). Therefore, BEST-WR produced considerably lower relative error values in comparison to BEST, revealing a substantially higher prediction ability of the proposed method. More specifically, for the case of concave-shaped curves (high α_{WR} values), both methods yielded low $|Er(S)|$ and $|Er(K_s)|$ values. These results suggest that Eqs. (7) and (4a) provide similar results for hydrophilic soils and that the proposed method can also be applied to hydrophilic soils. For the case of convex-shaped curves (low α_{WR} values), the discrepancy between the two methods become relevant, and only BEST-WR provided a proper estimation of the soil hydraulic properties (S and K_s). In other words, BEST-WR applies to both water-repellent and hydrophilic soils. Therefore, we can conclude that, theoretically, the application of BEST-WR to hydrophilic soils should not affect the quality of the estimates for sorptivity and saturated hydraulic conductivity and that the proposed model should apply to all cases.

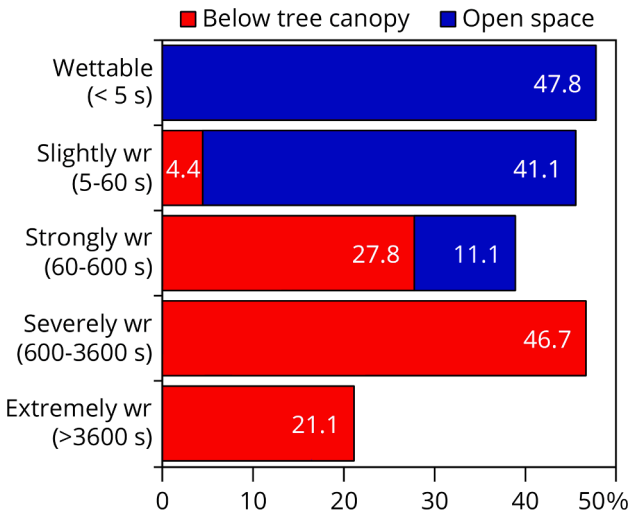

Fig. 4. Classification of the 180 WDPT tests carried out below the tree canopies (90 drops) and in the open spaces (90 drops) in five repellency classes according to the criterion proposed by Dekker and Ritsema (1994).

4.2. *Assessing soil water repellency in a Mediterranean wooded grassland system*

Both the α_{WR} parameter and WDPT were non-normally distributed according to the Kolmogorov-Smirnov test, even if log-transformed. Thus, we used the non-parametric Kruskal-Wallis test to determine whether the medians of two groups (open space and below tree canopy) were different.

In the open spaces, the WDPT values ranged between 1 and 259 s, with a median value equal to 5 s. Below the tree canopies, the median WDPT value was 1404 s, with 19 out of 90 drops (21%) that lasted >3600 s to infiltrate. According to the Kruskal-Wallis test the two medians were significantly different ($P < 0.05$), with higher WDPT values below the canopies as compared to the open spaces. According to the classification proposed by Dekker and Ritsema (1994), the WDPT values were grouped in five classes from wettable (WDPT < 5 s) to extremely water-repellent (WDPT > 3600 s) (Fig. 4). Wettable conditions were only found in the open spaces, with 47.8% of the drops that infiltrated in <5 s. Here, the 41.1 % of the tests were classified as slightly water

Table 4
Sample size (N), minimum (min), maximum (max), median, and standard deviation (SD) of the α_{WR} parameter, and water drop penetration time, WDPT, for the tests carried below the tree canopies and the in open spaces.

Location	N	min	max	median	SD
	α_{WR} (h^{-1})				
Open space	30	1.4	1364.2	12.7 A	271.1
Below tree canopy	30	0.5	320.5	6.6B	59.6
	WDPT (s)				
Open space	90	1	259	5B	44.6
Below tree canopy	90	10	>3600	1404 A	1306.7

For a given variable, different letters represent significant differences according to the non-parametric Kruskal-Wallis test ($P < 0.05$).

repellent and the 11.1 % as strongly water repellent. Below the tree canopies prevailed water repellent conditions, with the 21.1 % of the drops that lasted >3600 s to infiltrate (extremely water repellent). 46.7 % of the tests were classified severely water-repellent, 27.8 % as strongly water-repellent and 4.4 % as slightly water-repellent. Thus, below the tree canopies, and for initially dry conditions, phenomena of flow impedance are expected to be stronger as compared to the open spaces. However, this type of test could be insufficient to gain a comprehensive understanding of the hydraulic response of a water-repellent soil. Indeed, SWR can promote preferential flow and by-pass flow that cannot be detected by a drop scale measurement technique (e.g., Bachmann et al., 2003; Chen et al., 2020; Scott, 2000).

Compared to WDPT, α_{WR} includes information on flow dynamics, therefore, it can be considered more physically linked to the hydrological processes affected by water repellency. We then compared the values of α_{WR} to the values of WDPTs. In the open spaces, α_{WR} values ranged between 1.4 and 1364.2 h^{-1}, with a median value equal to 12.7 h^{-1}. According to the Kruskal-Wallis test, the α_{WR} values measured below the tree canopies were significantly lower (Table 4; Fig. 5), with values ranging from 0.5 to 320.5 h^{-1}, and a median value equal to 6.6 h^{-1}. Low α_{WR} values are associated with increased SWR effect and initially attenuated infiltration rates, which typically results in convex-shaped cumulative infiltration curves (Abou Najm et al., 2021). Thus, both α_{WR} and WDPT measurements revealed more noticeable soil water repellent phenomena below the canopies as compared to the open spaces. This likely because the higher soil organic carbon content in the 0–40-cm soil layer below the trees (Seddaiu et al., 2018). Previous studies also reported soil hydrophobicity below the canopies of Mediterranean oaks (Di Prima et al., 2017; Lozano-Parra et al., 2015).

4.3. Experimental assessment of BEST-WR

Given that intermediate water repellency conditions were found in both locations, i.e., below tree canopies and open spaces (Fig. 4), we decided to group the infiltration measurements based on the shape of the cumulative infiltration curves, which can reveal the occurrence of water repellent conditions (Angulo-Jaramillo et al., 2019). Three main types of shapes can be detected: i) regular shape with a concave part followed by a linear part (decreasing infiltration rate), which is associated with infiltration into hydrophilic mineral materials, ii) a typical convex (hockey-stick-like) relationship (increasing infiltration rate), which is associated with hydrophobic organic materials, and iii) a mixed shape (concave-then-convex) with a very small concave part followed by the hockey-stick-like shape (decreasing before increasing infiltration rate), this latter shape associated with weak water repellency phenomena due to fractional wettability (Angulo-Jaramillo et al., 2019). The impact of hydrophobicity on the shape of the cumulative infiltration influences BEST treatment of the data, leading to failed analysis due to a poor fit of the infiltration model and negative values for the saturated soil hydraulic conductivity (Di Prima et al., 2019; Lassabatere et al., 2019a). Specifically, measurements were grouped into three subsets: i) those that have a convex (hockey-stick-like) shape (43 runs out 60, 71.7%), ii) those that have a concave-then-convex shape (9 runs out 60, 15.0%), and iii) those that have a concave shape (8 runs out 60, 13.3%).

In the open spaces, 17 runs out 30 (56.7%) exhibited convex-shaped curves, while 7 (23.3%) had a concave-then-convex shape, and 6 (20.0%) were concave-shaped. Below the tree canopies, the number of convex-shaped curves increased to 26 out 30 (86.7%), while only 4 (13.3%) had concave-then-convex shapes or were concave-shaped (two for each type). This result confirms the observations done using WDPT data, that water repellent conditions were found in both locations, with more occurrences below the tree canopies.

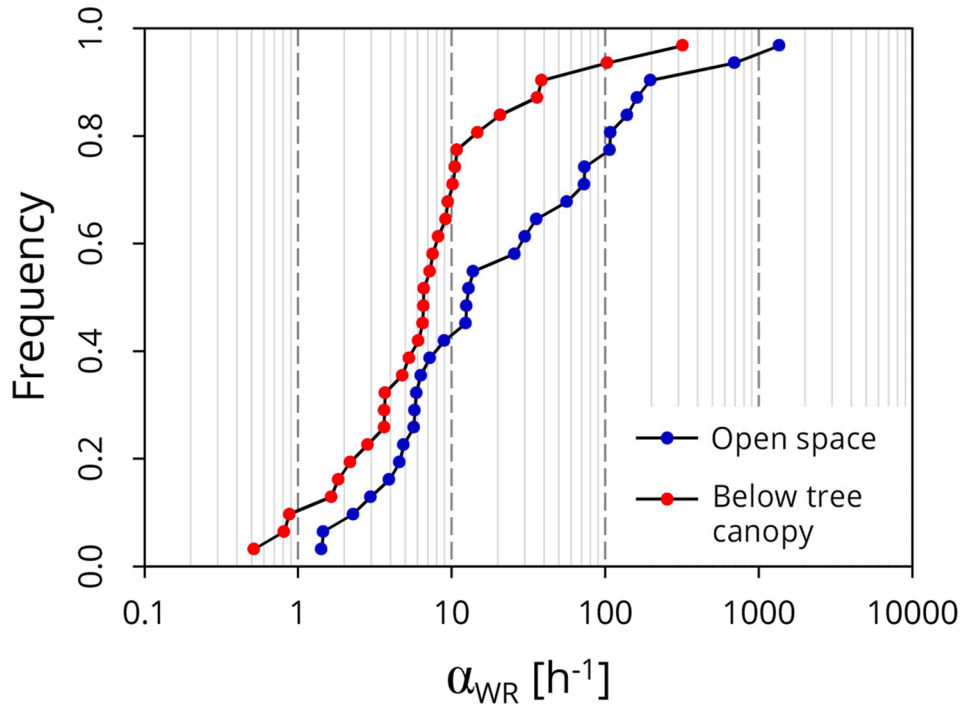

Fig. 5. Cumulative frequency distributions for the α_{WR} (h^{-1}) parameter, for infiltration measurements carried out below the tree canopies and in the open spaces.

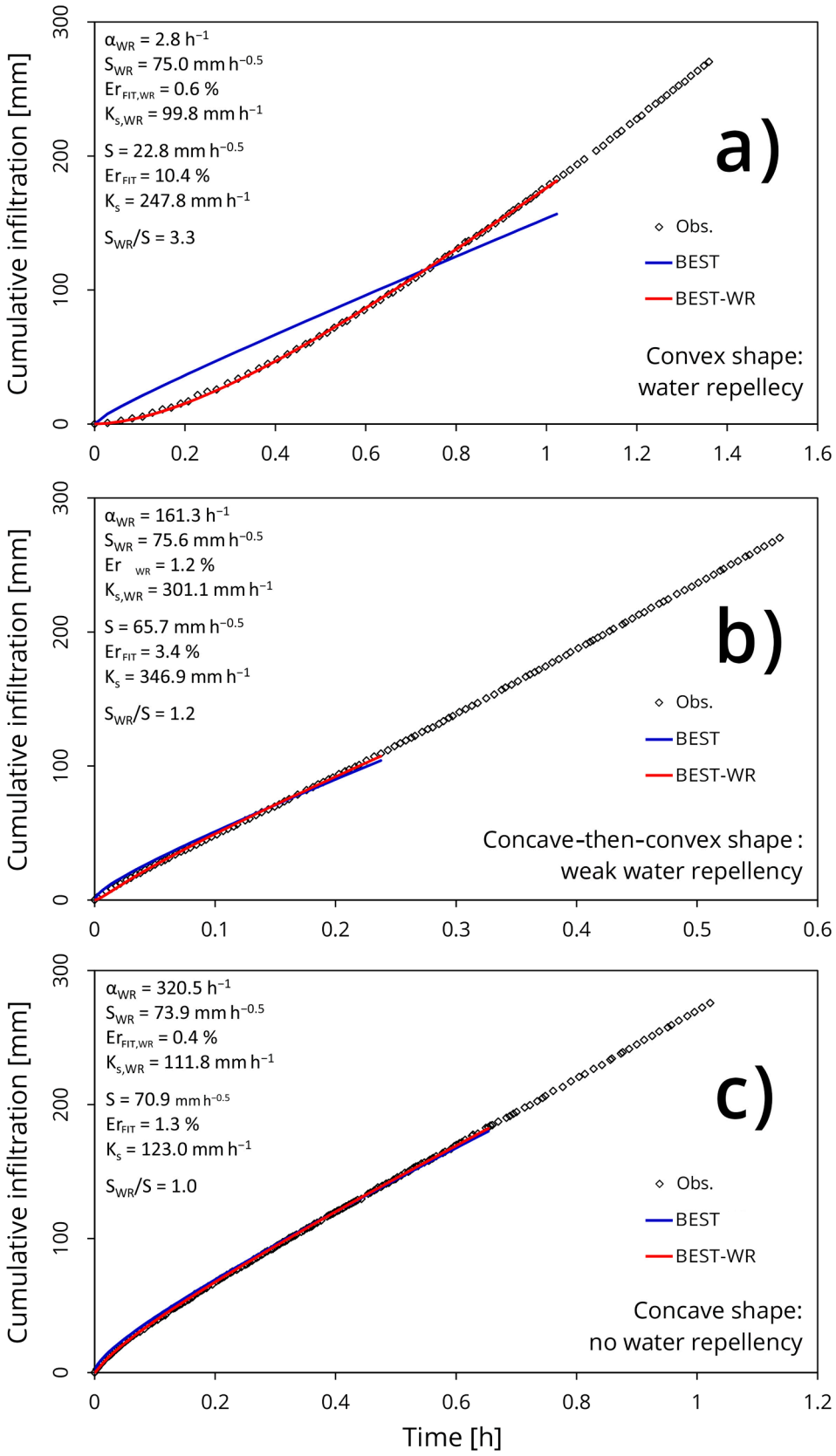

Fig. 6. Examples for convex (hockey-stick-like), concave-then-convex (mixed shape) and concave curves comparing experimental results from infiltration experiments (circles) to results from Eq. (4b) (blue) and Eq. (7) (red). (For interpretation of the references to colour in this figure legend, the reader is referred to the web version of this article.)

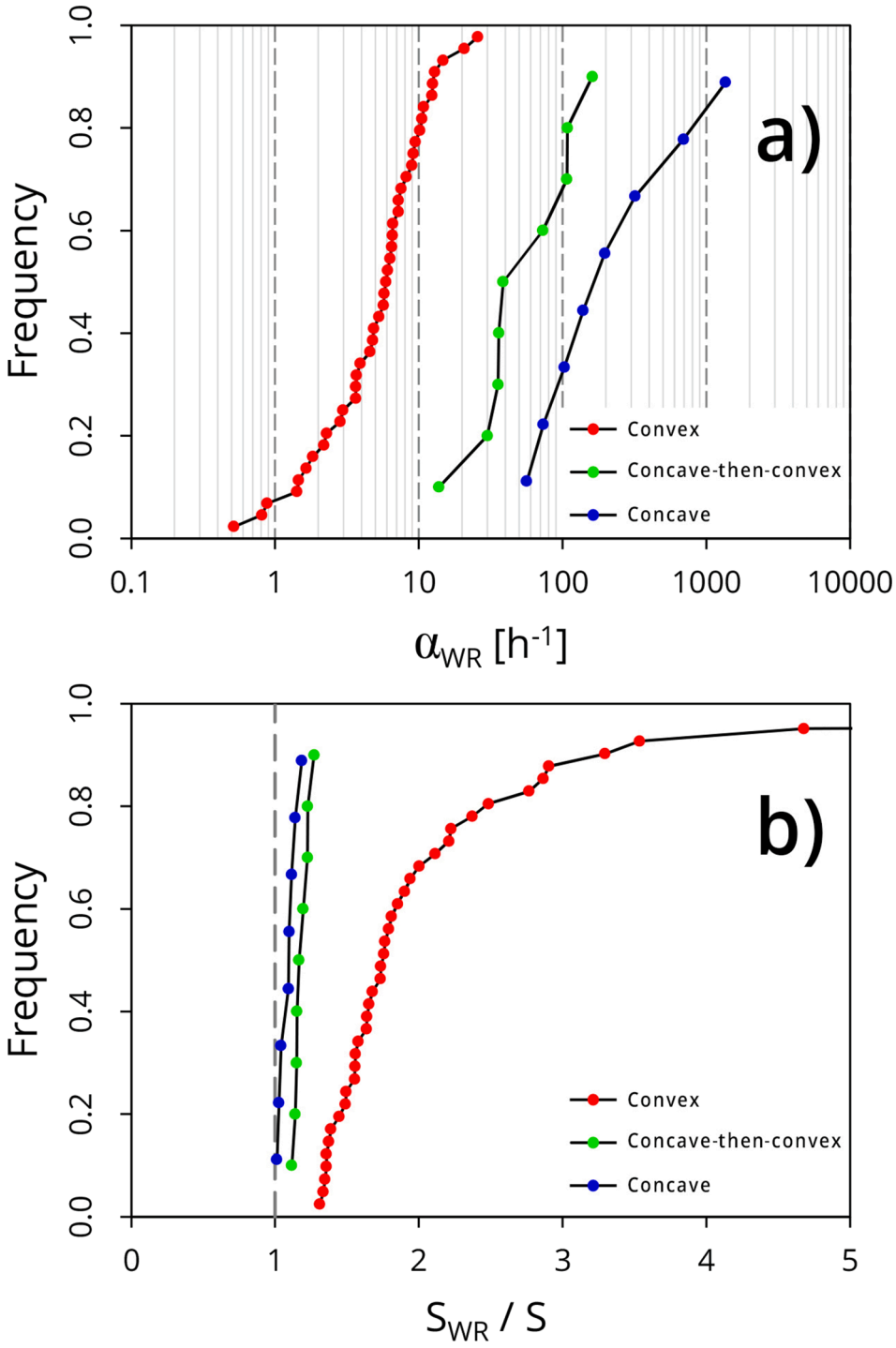

Fig. 7. Cumulative frequency distributions for a) α_{WR} (h^{-1}) parameter, and b) S_{WR}/S ratio for convex (hockey-stick-like), concave-then-convex and concave curves.

Fig. 6 shows three examples, one for each case. The **subpanel a** illustrates the case of a convex-shaped curve. This experiment has infiltration rates that increased with time, such that the cumulative infiltration curve exhibited a convex shape. For this run, the fitting of Eq. (7) produced a considerably lower relative error value in comparison to Eq. (4b), i.e., $Er_{FIT,WR} = 0.6\%$ against $Er_{FIT} = 10.4\%$, revealing a substantially higher fitting ability of the proposed model (Eq. (7)) adapted to convex-shaped data. The value of α_{WR} was equal to 2.8 h^{-1}, while the two values of soil sorptivity, S_{WR} and S, estimated fitting respectively Eqs. (7) and (4b) to the experimental data were equal to 75.0 and 22.8 mm $h^{-0.5}$, differing by a factor of 3.3.

For the cases of concave-then-convex shape (Fig. 6**b**) and concave-shaped (Fig. 6**c**) curves, we estimated higher α_{WR} values, because of the reduced effect of water repellency on the infiltration process. The discrepancies between the two models in terms of relative error, soil sorptivity and saturated soil hydraulic conductivity were less noticeable for the case of weak water repellency (Fig. 6**b**), or even negligible when the experiment was not affected at all (Fig. 6**c**). Indeed, for this latter case, we estimated almost the same values of soil sorptivity, with S_{WR} and S equal respectively to 73.9 and 70.9 mm $h^{-0.5}$, and low fitting relative error values in both cases.

These results suggest that Eqs. (7) and (4b) provide the same result in

Table 5
Sample size (N), minimum (min), maximum (max), geometric mean (GM), and geometric coefficient of variation (GCV, %) of the soil sorptivity, S_{WR} (mm $h^{-0.5}$), and the saturated soil hydraulic conductivity, $K_{s,WR}$ (mm h^{-1}), for different shapes of the cumulative infiltration $I(t)$.

Variable	Shape of $I(t)$	N	min	max	GM	GCV
S_{WR}	Convex	43	30.2	157.9	55.0 A	31
	Concave than convex shape	9	37.1	100.4	62.4 A	36
	Hockey-stick-like	8	25.3	126.1	70.5 A	51
$K_{s,WR}$	Convex	42	13.1	259.7	106.1 A	72
	Concave than convex shape	9	59.8	380.6	154.2 A	69
	Hockey-stick-like	8	42.0	272.9	98.1 A	63

For a given variable, means followed by the same letter were not significantly different according to the Tukey's Honestly Significant Difference test ($P < 0.05$).

Table 6
Sample size (N), minimum (min), maximum (max), mean and coefficient of variation (CV, %) of the saturated soil hydraulic conductivity, K_s (mm h^{-1}), van Genuchten pressure scale parameter, α_{vG} (mm^{-1}), saturated volumetric soil water content (θ_s in m^3 m^{-3}), and hydraulic shape parameters, n, m, and η (estimated from the PSDs according to Lassabatere et al. (2006)), measured below the tree canopies and in the open spaces at the Berchidda site.

Variable	Location	N	min	max	mean	CV
[†]K_s (mm h^{-1})	Open space	30	42.0	380.6	104.8 A[††]	62.5
	Below tree canopy	29	13.1	259.7	121.0 A	54.7
α_{vG} (%)	Open space	30	0.007	0.050	0.028 a	38.8
	Below tree canopy	29	0.003	0.069	0.030 a	47.7
θ_s (m^3 m^{-3})	Open Space	9	0.373	0.458	0.415 b	5.5
	Below tree canopy	9	0.454	0.543	0.489 a	6.0
n (−)	Open space	9	2.194	2.256	2.217 a	0.8
	Below tree canopy	9	2.197	2.279	2.220 a	1.2
m (−)	Open space	9	0.089	0.113	0.098 a	7.7
	Below tree canopy	9	0.090	0.122	0.099 a	10.6
η (−)	Open space	9	10.8	13.3	12.3 a	6.2
	Below tree canopy	9	10.2	13.1	12.2 a	7.9

For all the other variables, means followed by the same low case letter were not significantly different, while means followed by different low case letter were significantly different according to the two-sample t-test ($P < 0.05$).

[†] According to the Kolmogorov-Smirnov test, both non-transformed and log-transformed K_s data were non-normally distributed, thus, the median was calculated for this variable. The arithmetic mean was calculated for all the other variables.

[††] For K_s, the same upper case letters represent not significant differences according to the non-parametric Kruskal-Wallis test ($P < 0.05$).

case of hydrophilic soils. However, only the new proposed model Eq. (7) can provide a satisfactory fitting and a proper estimation of the soil hydraulic properties (S and K_s) when water repellency occurs, i.e., for the case of convex-shaped curves. In other words, this result supports the same conclusions stated above for the analytical validation, i.e., that BEST-WR applies to both water-repellent and hydrophilic soils.

These observations can be generalized to all the infiltration measurements. Fig. 7**a** illustrates the discrepancy between α_{WR} values associated with different shapes of the cumulative infiltration curves and, thus, with the relevance of water repellency phenomena at the soil surface. A similarity between sorptivity values were always found for weak or no repellency conditions (Fig. 7**b**, S_{WR}/S close to unity). Otherwise, the discrepancy between the two estimations become relevant for convex-shaped curves.

A remarkable result is that Eq. (7) provided similar soil hydraulic properties (S and K_s) for the three cases, independently from the shape of

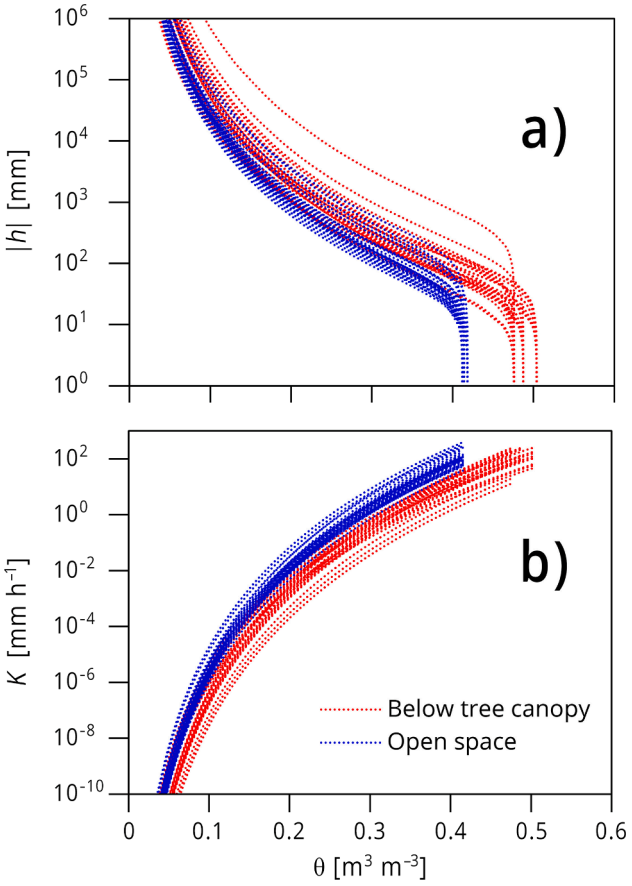

Fig. 8. (**a**) Water retention curves, $\theta(h)$, and (**b**) soil hydraulic conductivity functions, $K(\theta)$, predicted by BEST-WR at the two locations: below the tree canopies and in the open spaces.

the curves (Table 5). Taken together, these findings suggest that the correction factor can quantify the effect of water repellency at the soil surface without impacting the physical model used, so that infiltration continues to be quantified using common soil hydraulic properties. The results obtained here can be viewed as a confirmation of the conclusion by Abou Najm et al. (2021). Now, there remains the question of the meaning of α_{WR}. Does it correspond to an intrinsic parameter, or otherwise a macroscopic parameter that depends at the same time on the soil features (in terms of organic matter, etc.) and on initial conditions (water content and type of application of water)?

4.4. Hydraulic characterization through BEST-WR of the soils below the tree canopies and in the grassland

BEST-WR allowed to estimate the scale (θ_s, K_s, and α_{vG}) and shape (n, m and η) parameters of the soil characteristics curves (Table 6). Once S and K_s were estimated with Eq. (7), the remaining parameters were estimated in the same way as for BEST-Slope (Lassabatere et al., 2006). While the scale parameters were determined by modeling infiltration data through Eq. (7), the shape parameters were estimated from the PSD analysis according to the procedure developed in Lassabatere et al. (2006)). The hydraulic shape parameters for the two locations were similar due to their similar textures (Table 6). Among the scale parameters, only θ_s differed between the two locations, because of the lower bulk density values measured below the tree canopies (Table 3). Fig. 8 shows for the two locations the water retention and hydraulic conductivity curves predicted by BEST-WR. The water retention curves are presented with water content as a function of water pressure head with log scale (Fig. 8**a**). The hydraulic conductivity was plotted with log scale

as a function of water content (Fig. 8**b**). The curves measured below the tree canopies are more positioned on the right, namely the water content corresponding to a given pressure head is generally higher for these curves as compared to the open space, indicating higher capillarity effects (Fig. 8**a**). For this location, the hydraulic conductivity functions are positioned below in the graph, namely the hydraulic conductivity corresponding to a given water content is generally lower as compared to the open space, indicating a lower capacity to conduct water under unsaturated conditions, although, under saturated condition, the hydraulic conductivity is similar for the two locations (Table 6).

A higher capacity to retain water by capillarity below the tree canopies can be viewed as a mechanism of soil moisture capture that increases the storage capacity of patchy areas within the wooded grassland system (Naveed et al., 2019). In addition, these patches are less susceptible to soil evaporation losses due to the shadow of the canopies and the presence of a surface water repellent layer (Robinson et al., 2010). During the summer drought, this may constitute a competitive advantage for the scattered trees, with more water available for the trees as compared to the open grassland.

5. Summary and conclusions

In this investigation, we presented an adaptation of the BEST method, named BEST-WR, for the hydraulic characterization of both hydrophilic and water-repellent soils. We validated the proposed method using both analytically generated data and infiltration experiments carried out in a Mediterranean wooded grassland, where the scattered evergreen oak trees induced soil water repellency under the canopies. The analytical validation and the field measurements supported our hypothesis that the modified Haverkamp model (Eq. (7)), included in BEST-WR, is suitable to predict S and K_s under both hydrophilic and water-repellent conditions. Eqs. (7) and (4b) provided similar results only for the case of hydrophilic soils (concave-shaped curves). Conversely, when water repellency occurred, only Eq. (7) provided satisfactory fittings and proper estimations of S and K_s. In addition, Eq. (7) proved to quantify the effect of water repellency at the soil surface without impacting the estimation of the soil hydraulic properties.

The use of α_{WR} as a new hydrological SWR index allowed us to detect more noticeable soil water repellent phenomena below the canopies as compared to the open grassland. These measurements were in line with those obtained using the WDPT test, which is one of the most widely test applied for quantifying SWR persistence. At the same time, BEST-WR succeeded in determining the soil characteristics curves. These curves evidenced a higher capacity to retain water by capillarity below the tree canopies, and highlighted how scattered trees can strongly influence ecohydrological processes and water dynamics within wooded grassland systems. Supported by these examples, we expect that the new method will allow researchers to better approach heterogeneous datasets, including data collected on both hydrophilic and water-repellent soils. The versatility of the new method makes it a good candidate to successfully analyze infiltration databases, as those developed by Rahmati et al. (2018) and Di Prima et al. (2020).

Funding

This work was supported through i) the European Regional Development Fund (ERDF) and the Italian Ministry of Education, University and Research (MIUR) through the “Programma Operativo Nazionale (PON) Ricerca e Innovazione 2014–2020 (Linea 1 - Mobilità dei ricercatoriAIM1853149, CUP: J54I18000120001), ii) GASPAM Gestione Agronomica sostenibile dei pascoli arborati mediterranei. Regione Sardegna, L. 7/2007, 2019–21, iii) the INFILTRON Project (ANR-17-CE04-0010, Package for assessing infiltration & filtration functions of urban soils in stormwater management; https://infiltron.org/), and iv) the “fondo di Ateneo per la ricerca 2020” of the University of Sassari.

CRediT authorship contribution statement

Simone Di Prima: Conceptualization, Methodology, Investigation, Formal analysis, Validation, Visualization, Writing - original draft, Writing - review & editing, Funding acquisition. **Ryan D. Stewart:** Conceptualization, Methodology, Writing - review & editing. **Majdi R. Abou Najm:** Conceptualization, Methodology, Writing - review & editing. **Ludmila Ribeiro Roder:** Investigation, Data curation, Writing - review & editing. **Filippo Giadrossich:** Investigation. **Sergio Campus:** Investigation. **Rafael Angulo-Jaramillo:** Writing - review & editing. **Deniz Yilmaz:** Validation, Writing - review & editing. **Pier Paolo Roggero:** Writing - review & editing, Funding acquisition. **Mario Pirastru:** Writing - review & editing. **Laurent Lassabatere:** Conceptualization, Methodology, Writing - review & editing, Funding acquisition.

Declaration of Competing Interest

The authors declare that they have no known competing financial interests or personal relationships that could have appeared to influence the work reported in this paper.

References

Abou Najm, M.R., Stewart, R.D., Di Prima, S., Lassabatere, L., 2021. A simple correction term to model infiltration in water-repellent soils. Water Resour. Res. 57 (2) https://doi.org/10.1029/2020WR028539.

Alagna, V., Iovino, M., Bagarello, V., Mataix-Solera, J., Lichner, L., 2019. Alternative analysis of transient infiltration experiment to estimate soil water repellency. Hydrol. Process. 33 (4), 661–674. https://doi.org/10.1002/hyp.v33.410.1002/hyp.13352.

Angulo-Jaramillo, R., Bagarello, V., Di Prima, S., Gosset, A., Iovino, M., Lassabatere, L., 2019. Beerkan Estimation of Soil Transfer parameters (BEST) across soils and scales. J. Hydrol. 576, 239–261. https://doi.org/10.1016/j.jhydrol.2019.06.007.

Angulo-Jaramillo, R., Bagarello, V., Iovino, M., Lassabatere, L., 2016. Saturated Soil Hydraulic Conductivity, in: Infiltration Measurements for Soil Hydraulic Characterization. Springer International Publishing, pp. 43–180. https://doi.org/10.1007/978-3-319-31788-5_2.

Bachmann, J., Woche, S.K., Goebel, M.-O., Kirkham, M.B., Horton, R., 2003. Extended methodology for determining wetting properties of porous media. Water Resour. Res. 39, 1353. https://doi.org/10.1029/2003WR002143.

Bagarello, V., Castellini, M., Di Prima, S., Iovino, M., 2014a. Soil hydraulic properties determined by infiltration experiments and different heights of water pouring. Geoderma 213, 492–501. https://doi.org/10.1016/j.geoderma.2013.08.032.

Bagarello, V., Di Prima, S., Iovino, M., 2014b. Comparing Alternative Algorithms to Analyze the Beerkan Infiltration Experiment. Soil Sci. Soc. Am. J. 78 (3), 724–736. https://doi.org/10.2136/sssaj2013.06.0231.

Bagarello, V., Di Prima, S., Iovino, M., Provenzano, G., 2014c. Estimating field-saturated soil hydraulic conductivity by a simplified Beerkan infiltration experiment. Hydrol. Process. 28 (3), 1095–1103. https://doi.org/10.1002/hyp.v28.310.1002/hyp.9649.

Bagarello, V., Iovino, M., Reynolds, W., 1999. Measuring hydraulic conductivity in a cracking clay soil using the Guelph permeameter. Trans ASAE 42.

Bagella, S., Caria, M.C., Farris, E., Rossetti, I., Filigheddu, R., 2016. Traditional land uses enhanced plant biodiversity in a Mediterranean agro-silvo-pastoral system. Plant Biosyst. – Int. J. Dealing Aspects Plant Biol. 150 (2), 201–207. https://doi.org/10.1080/11263504.2014.943319.

Bagella, S., Caria, M.C., Seddaiu, G., Leites, L., Roggero, P.P., 2020. Patchy landscapes support more plant diversity and ecosystem services than wood grasslands in Mediterranean silvopastoral agroforestry systems. Agric. Syst. 185, 102945. https://doi.org/10.1016/j.agsy.2020.102945.

Beatty, S.M., Smith, J.E., 2013. Dynamic soil water repellency and infiltration in post-wildfire soils. Geoderma 192, 160–172. https://doi.org/10.1016/j.geoderma.2012.08.012.

Braud, I., De Condappa, D., Soria, J.M., Haverkamp, R., Angulo-Jaramillo, R., Galle, S., Vauclin, M., 2005. Use of scaled forms of the infiltration equation for the estimation of unsaturated soil hydraulic properties (the Beerkan method). Eur. J. Soil Sci. 56 (3), 361–374. https://doi.org/10.1111/ejs.2005.56.issue-310.1111/j.1365-2389.2004.00660.x.

Brooks, R.H., Corey, T., 1964. Hydraulic properties of porous media. Hydrol. Paper 3. Colorado State University, Fort Collins.

Buczko, U., Bens, O., Hüttl, R.F., 2006. Water infiltration and hydrophobicity in forest soils of a pine–beech transformation chronosequence. J. Hydrol. 331 (3-4), 383–395. https://doi.org/10.1016/j.jhydrol.2006.05.023.

Burdine, N.T., 1953. Relative permeability calculation from pore size distribution data. Petr. Trans. Am Inst. Min. Metall. Eng. 198, 71–77.

Campbell, S.L., Chancelier, J.-P., Nikoukhah, R., 2010. Modeling and Simulation in Scilab/Scicos with ScicosLab 4.4, 2nd ed. Springer-Verlag, New York.

Carsel, R.F., Parrish, R.S., 1988. Developing joint probability distributions of soil water retention characteristics. Water Resour. Res. 24 (5), 755–769. https://doi.org/10.1029/WR024i005p00755.

Chen, J., McGuire, K.J., Stewart, R.D., 2020. Effect of soil water-repellent layer depth on post-wildfire hydrological processes. Hydrol. Process. 34 (2), 270–283. https://doi.org/10.1002/hyp.v34.210.1002/hyp.13583.

Concialdi, P., Di Prima, S., Bhanderi, H.M., Stewart, R.D., Abou Najm, M.R., Lal Gaur, M., Angulo-Jaramillo, R., Lassabatere, L., 2020. An open-source instrumentation package for intensive soil hydraulic characterization. J. Hydrol. 582, 124492. https://doi.org/10.1016/j.jhydrol.2019.124492.

Dekker, L.W., Ritsema, C.J., 1994. How water moves in a water repellent sandy soil: 1. Potential and actual water repellency. Water Resour. Res. 30 (9), 2507–2517. https://doi.org/10.1029/94WR00749.

Di Prima, S., 2019. An open source instrumentation package for intensive soil hydraulic characterization [https://www.youtube.com/watch?v=KW1zLcuDQg8].

Di Prima, S., 2015. Automated single ring infiltrometer with a low-cost microcontroller circuit. Comput. Electron. Agric. 118, 390–395. https://doi.org/10.1016/j.compag.2015.09.022.

Di Prima, S., Bagarello, V., Angulo-Jaramillo, R., Bautista, I., Cerdà, A., del Campo, A., González-Sanchis, M., Iovino, M., Lassabatere, L., Maetzke, F., 2017. Impacts of thinning of a Mediterranean oak forest on soil properties influencing water infiltration. J. Hydrol. Hydromech. 65, 276–286. https://doi.org/10.1515/johh-2017-0016.

Di Prima, S., Castellini, M., Abou Najm, M.R., Stewart, R.D., Angulo-Jaramillo, R., Winiarski, T., Lassabatere, L., 2019. Experimental assessment of a new comprehensive model for single ring infiltration data. J. Hydrol. 573, 937–951. https://doi.org/10.1016/j.jhydrol.2019.03.077.

Di Prima, S., Lassabatere, L., Bagarello, V., Iovino, M., Angulo-Jaramillo, R., 2016. Testing a new automated single ring infiltrometer for Beerkan infiltration experiments. Geoderma 262, 20–34. https://doi.org/10.1016/j.geoderma.2015.08.006.

Di Prima, S., Stewart, R.D., Castellini, M., Bagarello, V., Abou Najm, M.R., Pirastru, M., Giadrossich, F., Iovino, M., Angulo-Jaramillo, R., Lassabatere, L., 2020. Estimating the macroscopic capillary length from Beerkan infiltration experiments and its impact on saturated soil hydraulic conductivity predictions. J. Hydrol. 589, 125159. https://doi.org/10.1016/j.jhydrol.2020.125159.

Doerr, S.H., Shakesby, R.A., Walsh, R.P.D., 2000. Soil water repellency: its causes, characteristics and hydro-geomorphological significance. Earth Sci. Rev. 51 (1-4), 33–65.

Gee, G.W., Bauder, J.W., 1986. Particle-size Analysis. Methods of Soil Analysis, Part 1: Physical and Mineralogical Methods. Soil Science Society of America, American Society of Agronomy, pp. 383–411.

Haverkamp, R., Parlange, J.-Y., Starr, J.L., Schmitz, G., Fuentes, C., 1990. Infiltration under ponded conditions: 3. A predictive equation based on physical parameters. Soil Sci. 149 (5), 292–300. https://doi.org/10.1097/00010694-199005000-00006.

Haverkamp, R., Ross, P.J., Smettem, K.R.J., Parlange, J.Y., 1994. Three-dimensional analysis of infiltration from the disc infiltrometer: 2. Physically based infiltration equation. Water Resour. Res. 30 (11), 2931–2935. https://doi.org/10.1029/94WR01788.

Hinnell, A.C., Lazarovitch, N., Warrick, A.W., 2009. Explicit infiltration function for boreholes under constant head conditions. Water Resour. Res. 45 (10) https://doi.org/10.1029/2008WR007685.

Iovino, M., Pekárová, P., Hallett, P.D., Pekár, J., Lichner, Ľ., Mataix-Solera, J., Alagna, V., Walsh, R., Raffan, A., Schacht, K., Rodný, M., 2018. Extent and persistence of soil water repellency induced by pines in different geographic regions. J. Hydrol. Hydromech. 66, 360–368. https://doi.org/10.2478/johh-2018-0024.

Jarvis, N., Etana, A., Stagnitti, F., 2008. Water repellency, near-saturated infiltration and preferential solute transport in a macroporous clay soil. Geoderma 143 (3-4), 223–230. https://doi.org/10.1016/j.geoderma.2007.11.015.

Lassabatere, L., Angulo-Jaramillo, R., Soria Ugalde, J.M., Cuenca, R., Braud, I., Haverkamp, R., 2006. Beerkan estimation of soil transfer parameters through infiltration experiments—BEST. Soil Sci. Soc. Am. J. 70 (2), 521–532. https://doi.org/10.2136/sssaj2005.0026.

Lassabatere, L., Di Prima, S., Angulo-Jaramillo, R., Keesstra, S., Salesa, D., 2019a. Beerkan multi-runs for characterizing water infiltration and spatial variability of soil hydraulic properties across scales. Hydrol. Sci. J. 64 (2), 165–178. https://doi.org/10.1080/02626667.2018.1560448.

Lassabatere, L., Di Prima, S., Bouarafa, S., Iovino, M., Bagarello, V., Angulo-Jaramillo, R., 2019b. BEST-2K Method for Characterizing Dual-Permeability Unsaturated Soils with Ponded and Tension Infiltrometers. Vadose Zone J. 18 (1), 1–20. https://doi.org/10.2136/vzj2018.06.0124.

Lassabatere, L., Peyneau, P.-E., Yilmaz, D., Pollacco, J., Fernández-Gálvez, J., Latorre, B., Moret-Fernández, D., Di Prima, S., Rahmati, M., Stewart, R.D., Abou Najm, M., Hammecker, C., Angulo-Jaramillo, R., 2021. Scaling procedure for straightforward computation of sorptivity. Hydrol. Earth Syst. Sci. Discuss. 1–33 https://doi.org/10.5194/hess-2021-150.

Lichner, L., Hallett, P.D., Drongová, Z., Czachor, H., Kovacik, L., Mataix-Solera, J., Homolák, M., 2013. Algae influence the hydrophysical parameters of a sandy soil. CATENA 108, 58–68. https://doi.org/10.1016/j.catena.2012.02.016.

Loizeau, S., Rossier, Y., Gaudet, J.-P., Refloch, A., Besnard, K., Angulo-Jaramillo, R., Lassabatere, L., 2017. Water infiltration in an aquifer recharge basin affected by temperature and air entrapment. J. Hydrol. Hydromech. 65, 222–233. https://doi.org/10.1515/johh-2017-0010.

Lozano-Parra, J., Schnabel, S., Ceballos-Barbancho, A., 2015. The role of vegetation covers on soil wetting processes at rainfall event scale in scattered tree woodland of Mediterranean climate. J. Hydrol. 529, 951–961. https://doi.org/10.1016/j.jhydrol.2015.09.018.

Minasny, B., McBratney, A.B., 2007. Estimating the Water Retention Shape Parameter from Sand and Clay Content. Soil Sci. Soc. Am. J. 71 (4), 1105–1110. https://doi.org/10.2136/sssaj2006.0298N.

Mualem, Y., 1976. A new model for predicting the hydraulic conductivity of unsaturated porous media. Water Resour. Res. 12 (3), 513–522.

Naveed, M., Ahmed, M.A., Benard, P., Brown, L.K., George, T.S., Bengough, A.G., Roose, T., Koebernick, N., Hallett, P.D., 2019. Surface tension, rheology and hydrophobicity of rhizodeposits and seed mucilage influence soil water retention and hysteresis. Plant Soil 437 (1-2), 65–81. https://doi.org/10.1007/s11104-019-03939-9.

Parlange, J.-Y., 1975. Convergence and validity of time expansion solutions: a comparison to exact and approximate solutions. Soil Sci. Soc. Am. J. 39, 3–6.

Rahmati, M., Weihermüller, L., Vanderborght, J., Pachepsky, Y.A., Mao, L., Sadeghi, S. H., Moosavi, N., Kheirfam, H., Montzka, C., Looy, K.V., Toth, B., Hazbavi, Z., Yamani, W.A., Albalasmeh, A.A., Alghzawi, M.Z., Angulo-Jaramillo, R., Antonino, A. C.D., Arampatzis, G., Armindo, R.A., Asadi, H., Bamutaze, Y., Batlle-Aguilar, J., Bechet, B., Becker, F., Blöschl, G., Bohne, K., Braud, I., Castellano, C., Cerdà, A., Chalhoub, M., Cichota, R., Císlerová, M., Clothier, B., Coquet, Y., Cornelis, W., Corradini, C., Coutinho, A.P., de Oliveira, M.B., de Macedo, J.R., Durães, M.F., Emami, H., Eskandari, I., Farajnia, A., Flammini, A., Fodor, N., Gharaibeh, M., Ghavimipanah, M.H., Ghezzehei, T.A., Giertz, S., Hatzigiannakis, E.G., Horn, R., Jiménez, J.J., Jacques, D., Keesstra, S.D., Kelishadi, H., Kiani-Harchegani, M., Kouselou, M., Kumar Jha, M., Lassabatere, L., Li, X., Liebig, M.A., Lichner, L., López, M.V., Machiwal, D., Mallants, D., Mallmann, M.S., Marques, O., De, J.D., Marshall, M.R., Mertens, J., Meunier, F., Mohammadi, M.H., Mohanty, B.P., Moncada, M.P., Montenegro, S., Morbidelli, R., Moret-Fernández, D., Moosavi, A.A., Mosaddeghi, M.R., Mousavi, S.B., Mozaffari, H., Nabiollahi, K., Neyshabouri, M.R., Ottoni, M.V., Filho, O., Benedicto, T., Rad, P., Reza, M., Panagopoulos, A., Peth, S., Peyneau, P.-E., Picciafuoco, T., Poesen, J., Pulido, M., Reinert, D.J., Reinsch, S., Rezaei, M., Roberts, F.P., Robinson, D., Rodrigo-Comino, J., Filho, R., Corrêa, O., Saito, T., Suganuma, H., Saltalippi, C., Sándor, R., Schütt, B., Seeger, M., Sepehrnia, N., Sharifi Moghaddam, E., Shukla, M., Shutaro, S., Sorando, R., Stanley, A.A., Strauss, P., Su, Z., Taghizadeh-Mehrjardi, R., Taguas, E., Teixeira, W. G., Vaezi, A.R., Vafakhah, M., Vogel, T., Vogeler, I., Votrubova, J., Werner, S., Winarski, T., Yilmaz, D., Young, M.H., Zacharias, S., Zeng, Y., Zhao, Y., Zhao, H., Vereecken, H., 2018. Development and Analysis of Soil Water Infiltration Global Database. Earth Syst. Sci. Data Discuss. 1–42 https://doi.org/10.5194/essd-10-1237-2018.

Reynolds, W.D., 2013. An assessment of borehole infiltration analyses for measuring field-saturated hydraulic conductivity in the vadose zone. Eng. Geol. 159, 119–130. https://doi.org/10.1016/j.enggeo.2013.02.006.

Robinson, D.A., Lebron, I., Ryel, R.J., Jones, S.B., 2010. Soil Water Repellency: A Method of Soil Moisture Sequestration in Pinyon–Juniper Woodland. Soil Sci. Soc. Am. J. 74 (2), 624–634. https://doi.org/10.2136/sssaj2009.0208.

Sándor, R., Iovino, M., Lichner, L., Alagna, V., Forster, D., Fraser, M., Kollár, J., Šurda, P., Nagy, V., Szabó, A., Fodor, N., 2021. Impact of climate, soil properties and grassland cover on soil water repellency. Geoderma 383, 114780. https://doi.org/10.1016/j.geoderma.2020.114780.

Scott, D.F., 2000. Soil wettability in forested catchments in South Africa; as measured by different methods and as affected by vegetation cover and soil characteristics. J. Hydrol. 231–232, 87–104. https://doi.org/10.1016/S0022-1694(00)00186-4.

Seddaiu, G., Bagella, S., Pulina, A., Cappai, C., Salis, L., Rossetti, I., Lai, R., Roggero, P.P., 2018. Mediterranean cork oak wooded grasslands: synergies and trade-offs between plant diversity, pasture production and soil carbon. Agroforest Syst. 92 (4), 893–908. https://doi.org/10.1007/s10457-018-0225-7.

Smettem, K.R.J., Parlange, J.Y., Ross, P.J., Haverkamp, R., 1994. Three-dimensional analysis of infiltration from the disc infiltrometer: 1. A capillary-based theory. Water Resour. Res. 30 (11), 2925–2929. https://doi.org/10.1029/94WR01787.

van Genuchten, M.T., 1980. A closed-form equation for predicting the hydraulic conductivity of unsaturated soils. Soil Sci. Soc. Am. J. 44 (5), 892–898.

Wessel, A.T., 1988. On using the effective contact angle and the water drop penetration time for classification of water repellency in dune soils. Earth Surf. Process. Landforms 13 (6), 555–561. https://doi.org/10.1002/(ISSN)1096-983710.1002/esp.v13:610.1002/esp.3290130609.

Xu, X., Lewis, C., Liu, W., Albertson, J.D., Kiely, G., 2012. Analysis of single-ring infiltrometer data for soil hydraulic properties estimation: Comparison of BEST and Wu methods. Agric. Water Manage. 107, 34–41. https://doi.org/10.1016/j.agwat.2012.01.004.

Yilmaz, D., Lassabatere, L., Angulo-Jaramillo, R., Deneele, D., Legret, M., 2010. Hydrodynamic Characterization of Basic Oxygen Furnace Slag through an Adapted BEST Method. Vadose Zone J. 9, 107. https://doi.org/10.2136/vzj2009.0039.